

Article

Dielectric Barrier Discharge Systems with HV Generators and Discharge Chambers for Surface Treatment and Decontamination of Organic Products

Jan Mucko ^{1,*} , Robert Dobosz ²  and Ryszard Strzelecki ³ 

¹ Faculty of Telecommunications, Computer Science and Electrical Engineering, UTP University of Science and Technology in Bydgoszcz, 85-796 Bydgoszcz, Poland

² Institute of Mathematics and Physics, UTP University of Science and Technology in Bydgoszcz, 85-796 Bydgoszcz, Poland; robertd@utp.edu.pl

³ Faculty of Electrical and Control Engineering, Gdańsk University of Technology, 80-233 Gdańsk, Poland; ryszard.strzelecki@pg.edu.pl

* Correspondence: mucko@utp.edu.pl; Tel.: +48-52-340-8511

Received: 3 September 2020; Accepted: 30 September 2020; Published: 5 October 2020



Abstract: The article presents applications of systems with power electronic converters, high voltage transformers, and discharge chambers used for nonthermal, dielectric barrier discharge plasma treatment of a plastic surface and decontamination of organic loose products. In these installations, the inductance of the high voltage transformers and the capacitances of the electrode sets form resonant circuits that are excited by inverters. The article presents characteristic features of the installations and basic mathematical relationships as well as the impact of individual parameters of system components. These converters with their output installations were designed, built, and tested by the authors. Some of the converters developed by the authors are manufactured and used in the industry.

Keywords: resonant inverter; dielectric barrier discharge; nonthermal plasma; treatment of plastic surface; decontamination of organic loose products

1. Introduction

Plasma systems and plasma treated materials are now commonly used. The cold, nonthermal plasma (NTP) is produced usually by high voltage (HV) electrical discharges. In nonthermal plasma, most of the electric energy is used to produce high-energy electrons, not to heat the gas. The electrons themselves do not treat the surface. The high-energy electrons (1–2 eV) excite electronic states of molecules, vibrational states, and provide molecular dissociation (oxygen at the most). Namely atomic oxygen and electronically excited molecules contribute to the surface treatment and pollution control. Cold plasma applications are very diverse. The main applications of NTP include surface modification of plastics [1–3], ozone generation [4,5], surface decontamination [6–11], sterilization of wounds and soil [12,13], toxic and harmful gas and sewage decomposition [14–20]. One of the methods of producing cold plasma is the dielectric barrier discharge (DBD). A number of studies present theoretical foundations of barrier discharges, including models of discharge chambers and their substitute schemes, analytical description of current and voltage waveforms, voltage-charge characteristics (the Lissajous figures) [21–24]. The article [21] additionally includes a review of the applications of DBD to high power CO₂ lasers, excimer based ultraviolet and fluorescent lamps and flat large-area plasma displays. Another important application of barrier discharges and corona discharges (CD) is the investigation of the ionic wind generation and examination of its results for the development of propulsion [25]. The use of both barrier and corona discharges when supplying a set of several

electrodes with alternating and direct voltage enables the creation of curtains from nonthermal plasma with a relatively large width of the air gap [26].

Many articles are focused on the development of high voltage generators that are components of DBD plasma systems. Depending on the application, the power of supplies ranges from single watts to hundreds of kilowatts. The choice of power and feed method is important for the operation of the DBD reactor and for the intensity of the reaction. The most common voltage waveform used to power DBD plasma reactors is the high voltage alternating current (AC) wave. In DBD reactors and in pulsed corona discharge reactors (PCD, without a dielectric layer) unipolar and bipolar voltage waves are used, sometimes a discontinuous wave with a prepolarization.

Already in 1857, Werner von Siemens reported on first experimental investigations with DBD. He applied a mechanical pulser (“Wagnerscher Hammer”) interrupting the primary winding circuit of the HV transformer as the high-voltage generator [27,28]. Another simple high-voltage generator for barrier discharges can consist of an autotransformer and a high-voltage transformer fed directly from the power grid of voltage frequency 50 or 60 Hz [3]. However, the high voltage delivered to the electrodes with a frequency of 50 or 60 Hz has a much higher value than the voltage with the increased frequency generated by an inverter. Very popular solutions are voltage source inverters (VSI), with unregulated or regulated input voltage and with high voltage transformers connected to the output [22,26,29–35]. These inverters can often have a full or half-bridge structure. When supplying a DBD system from an inverter the selection of the supply frequency is associated with the resonant frequency of the transformer inductances (and additional inductances if present) and electrode set capacities. Other generator designs are also used. Low power generators can be made as fly-back converters [22,25]. Bridge converters can be equipped with snubber circuits that reduce du/dt or di/dt when transistors are switching (on/off). An interesting solution is the full-bridge in which only one branch uses the LDR (coil, diode, resistor) circuit for di/dt reduction [36]. This solution may be useful if a pulse width modulation with phase shift (PS-PWM) control is used. An example of the multiresonant generator is presented in [37]. The transformer inductances and capacitances of the electrode set (together with an additional capacitor) form one resonant circuit. Another resonant circuit provides conditions for zero current switching (ZCS) off transistors. The paper [38] describes variations of a diagonal half-bridge resonant converter topology (with four diodes and two transistors), which can be used to produce a single-period AC sinusoidal waveform. The method allows power regulation within very wide limits and makes possible the precharge pulse generation for transformer magnetization and gap voltage symmetrization. The construction of a HV generator [39,40] that allows the production of voltage waves with many different shapes is also very interesting. It consists of a 24-level cascaded H-bridge inverter and works without an HV transformer. A transformerless HV generator for DBD plasma producing is described in [41]. In the abovementioned example, the HV generator uses the phenomenon of voltage increase in a circuit under serial resonance conditions. The topology of the inverters with additional AC intermediate resonant circuits has been presented in [42]. Depending on the AC intermediate circuits these generators are characterized by properties of the current or voltage sources. In case of operation as the current source, the DBD discharges were very stable and the system was insured against arc discharges in a natural way.

The basic control methods of high voltage alternating current (HVAC) generators that are used to generate DBD plasma are described in [29,30,43]. These are pulse amplitude modulation (PAM), pulse width modulation (PWM), phase shift-pulse width modulation (PS-PWM, PSC), pulse density modulation (PDM), and pulse frequency modulation (PFM). In [31,32], the hybrid control of PDM and PFM is described.

While the above articles provide a good overview of the fundamentals of DBD discharge, their applications and HV generators design, they do not discuss the impact of individual components parameters and control variables on the power of DBD discharges. The aim of the paper at hand is to fill the gap. The discussion focusses on the following parameters: inverter input voltage, inverter output voltage frequency, DBD discharge ignition voltage, resonant circuit parameters together with

the discharge chamber model parameters and transformer ratio. This article presents DBD generators and plasma reactors used for surface treatment of plastics and decontamination of loose organic materials, developed under the supervision of the authors. Generators are presented as well as entire technological devices.

The HV generators, which the authors designed, manufactured, and tested consist of power electronics converters: rectifier, DC/DC converter (if any), voltage-source inverter, and HV transformer. Transformer leakage inductances (and additional inductances if used) form a series resonant circuit with the capacities of the electrode sets. The resonant circuits create the conditions for soft switching, which is almost lossless. Thanks to the soft switching, the converters have high efficiency and generate little radio interference. Soft switching may appear as zero current switching (ZCS) or zero voltage switching (ZVS). The ZVS will be preferred in the analyzed systems, which is characterized by lower losses in the frequency and power range that the authors are interested in (up to about 100 kHz by 0.5 kW and about 25 kHz by 10 kW of rated power).

1.1. Power Electronics Converter Topology and Their Control Methods

The topology of the used power electronics converter is presented in Figure 1. Depending on the inverter control method and the assumed power and frequency range the step-down converter and/or HF resonant choke may be omitted. Then, only the transformer leakage inductances will perform the function of a resonant choke.

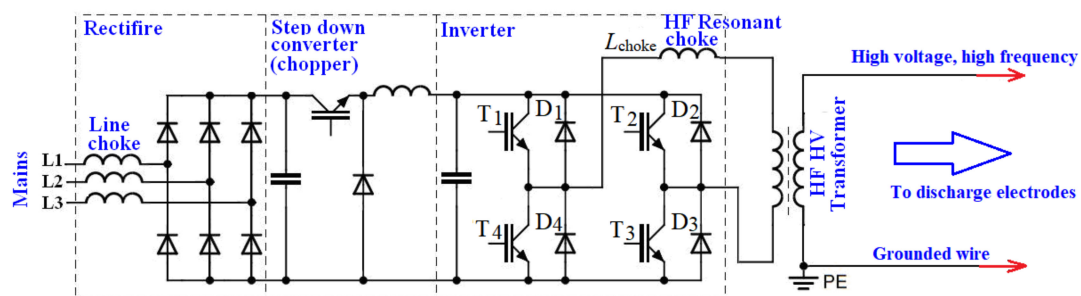


Figure 1. Schematic diagram of the power converter circuit used in the developed technological devices.

To control the output power of the converter, the following adjustment methods were considered [35]:

- pulse width modulation (PWM, with the constant inverter input voltage, the chopper can be omitted),
- changing the frequency of the inverter output (PFM, at constant inverter input voltage, the chopper can be omitted),
- changing the inverter input voltage (PAM, the chopper is necessary),
- PDM modulation (at constant inverter input voltage, the chopper can be omitted),
- combinations of the above methods.

Figure 2 shows the examples of the output current and voltage waveforms of the inverter with a series resonant circuit at the output for various analyzed control methods.

1.1.1. Output Power Control by Pulse Width Modulation, with Constant Inverter Input Voltage

Earlier studies and implementations carried out by one of the authors concerned the regulation of generator power using PWM. The chopper can be omitted to simplify the generator main circuit. This method is not recommended in the frequency range above several dozen (or even several) kHz and powers above a few kW. Turning off each of the transistors can be done “softly” (with appropriate transistors control) in the ZVS technique. However, switching on must be done “hard”. Hard commutation, at high switching frequency, causes significant losses and current stress caused by the sum of the load current and the reverse current of the inverter’s diodes (Figure 2a). In each half-period

of the output current, a reverse diode conducts then a transistor and then again reverse diode. There are six switching operations during the inverter operation period. This causes the inverter output voltage to oscillate at the frequency three times greater than the current wave. In the previously tested inverters, the transistors had to be oversized and the inverter was a strong source of radio frequency interference, also for its own control circuits.

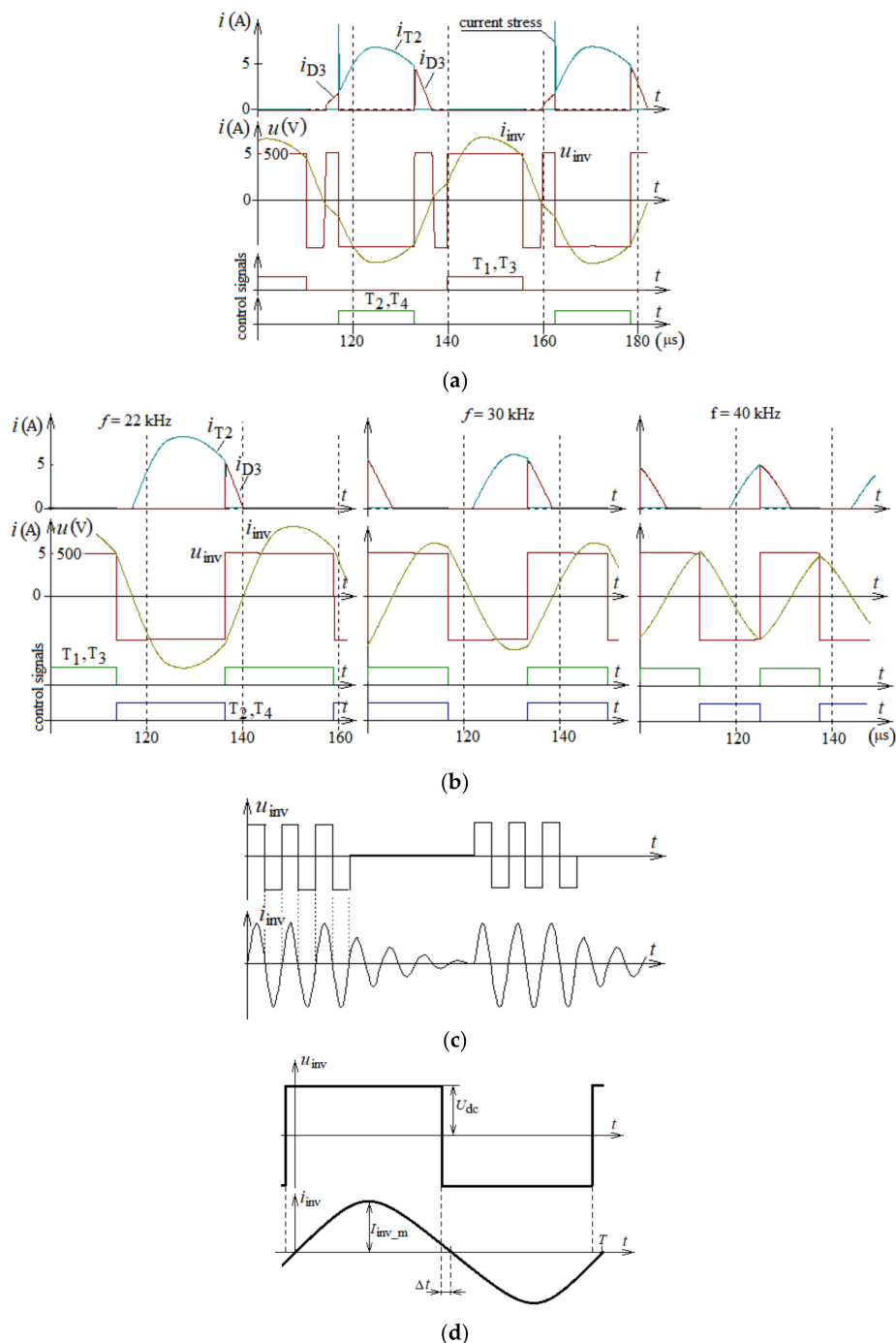


Figure 2. Waveforms of the inverter output voltage and current with different control methods, reproduced from Przegląd Elektrotechniczny [35]: (a) PWM, (b) PFM, (c) PDM, (d) PAM: i_T , i_D —transistor and diode current; i_{inv} —inverter output current; u_{inv} —inverter output voltage; for PWM, PDM, and PAM modulation it was assumed that the switching frequency is approximately equal to the resonant frequency and the voltage waveform is synchronized with the current in conditions for operation with ZVS switches.

Another kind of PWM modulation is the phase-shift pulse width modulation (PS-PWM, phase-shift control, PSC). In PS-PWM, transistors are conductive for half of the period and during diode conduction, the inverter output voltage is zero. This modulation has some advantages compared to PWM but also does not eliminate the hard switching in a wide range of power control [33,36].

1.1.2. Power Control by Pulse Frequency Modulation, with Constant Inverter Input Voltage

In this arrangement, the output power of the system is adjusted by changing the transistors switching frequency (Figure 2b). When operating below the resonant frequency, current stress in transistors occurs due to reverse currents of diodes. Thus, the authors do not recommend operating below the resonant frequency due to increased commutation losses. This method was previously used in series resonant inverters made in the thyristor technique. At the resonant frequency, the system works with maximum power. System operation (and power control) should take place at frequencies above resonance. Then ZVS conditions are created for the transistor's operation. The converter power circuit is relatively simple due to the unregulated DC voltage (no chopper). The inverter operation frequency should be limited both above and below so as not to go beyond the frequency range accepted in a given production process.

1.1.3. Power Control by Changing the Voltage at the Inverter Input

Earlier implementation carried out by one of the authors also considered regulation of generator power by changing the DC voltage supplying the inverter. This DC voltage source can be a controlled or semicontrolled thyristor rectifier, a noncontrolled rectifier with PFC converter or a transistor chopper (Figure 1). The system, although more complex, has a number of advantages. To enable the inverter transistors to work as ZVS switches, the transistors are turned off before the output current reaches zero. At the same time, if the switching frequency is close to the resonance frequency then the transistors turn off the low current. This is quasi-ZCS switching (Figure 2d). When ZVS and at the same time quasi-ZCS switching occurs, the inverter works in the most favorable conditions. Commutation losses are eliminated, and voltage and current steepness are limited. To ensure these optimal conditions it is necessary to automatically adjust the inverter switching frequency employing PLL. All power control processes take place in the chopper. Independent control of the inverter (PLL) and chopper is provided. Under these conditions, the time intervals at which energy returns to the DC source are very small. Then the amplitude, RMS, and average of the inverter output current (and transistor current) will be the lowest at the given output power. Assuming a sinusoidal current waveform and that $\Delta t \ll T_s$ (Figure 2d) one gets an approximate equation for the output power of the bridge inverters (Equation (1)):

$$P \approx \frac{1}{T_s/2} \int_0^{T_s/2} U_{dc} I_{inv_m} \sin(\omega_s t) dt = \frac{2U_{dc} I_{inv_m}}{\pi} \approx 0.9 U_{dc} I_{inv_RMS} \quad (1)$$

where: U_{dc} —DC inverter input voltage, I_{inv_m} , I_{inv_RMS} —maximum and RMS value of the inverter output current, T_s, f_s, ω_s —period, switching, and angular frequency.

1.1.4. Power Control by PDM Modulation (at Constant Inverter Input Voltage)

PDM modulation ensures even distribution of discharges over the entire length of the electrodes with a wide range of changes in average process power. The power regulation by means of PDM consists of sending in “packets” the maximum power with the frequency of a modulating generator with regulated filling [29,30,43]. The transistors in the inverter can work with ZVS soft commutation at a switching frequency greater than the resonant frequency. For maximum use of components (minimum transistors current in relation to the transferred power), the system should work with a frequency close to resonance. The general working principle is shown in Figure 2c. Turning off the “packet” is accomplished by switching on of two transistors T_1 and T_2 or T_3 and T_4 . Then the

oscillations in the resonant circuit go out automatically. The generator power circuit is relatively simple due to the unregulated DC voltage. The control system should also ensure that the transformer does not saturate, regardless of the length of the “packet” of power pulses and the pause time [43]. In particular, an even number of half-waves of the inverter output voltage should be maintained. During a break in power transfer, one must remember the switching frequency to which the system tuned during power flow. Assuming a sinusoidal current waveform and that $\Delta t \ll T_s$ (as in Figure 2c,d), one obtains the equation for the output power of the bridge inverter:

$$P \approx \frac{2U_{dc}I_{inv_m}}{\pi} D_{PDM} \approx 0.9U_{dc}I_{inv_RMS}D_{PDM} \quad (2)$$

where: D_{PDM} —duty cycle of PDM.

1.1.5. Author’s Method Based on Simultaneous PDM and PFM Modulation

The author’s method [24,44] based on simultaneous PDM and PFM modulation differs from the methods described in [31,32]. This control method was used in DBD discharge generators manufactured and used at the Institute of Polymer Materials and Dyes Engineering (IMPIB, Toruń, Poland) [45]. The essence of this control method is the combination of PDM and PFM modulation while the inverter operation is not stopped (switching off all transistors or short-circuit state of the load) but there is a periodic increase in the switching frequency (Figure 3). The range of frequency changes is limited from above and below according to the assumed maximum and minimum power. The PDM modulating signal can have a rectangular shape with variable (Figure 3a) or with fixed (Figure 3b) filling. Limiting the maximum power protects against damage to the processed material or arcing caused by a dielectric breakdown. This control method ensures uniform discharge in a wide range of power control (about 10–100% of nominal power) and has additional advantages over the classic PDM method [31,32]. The control system does not require the use of an additional system that remembers the frequency from the moment before the inverter stops and does not require a system counting the number of half-waves of the output voltage. Another advantage is the ease of modification of existing PFM control systems to work according to the proprietary method [24].

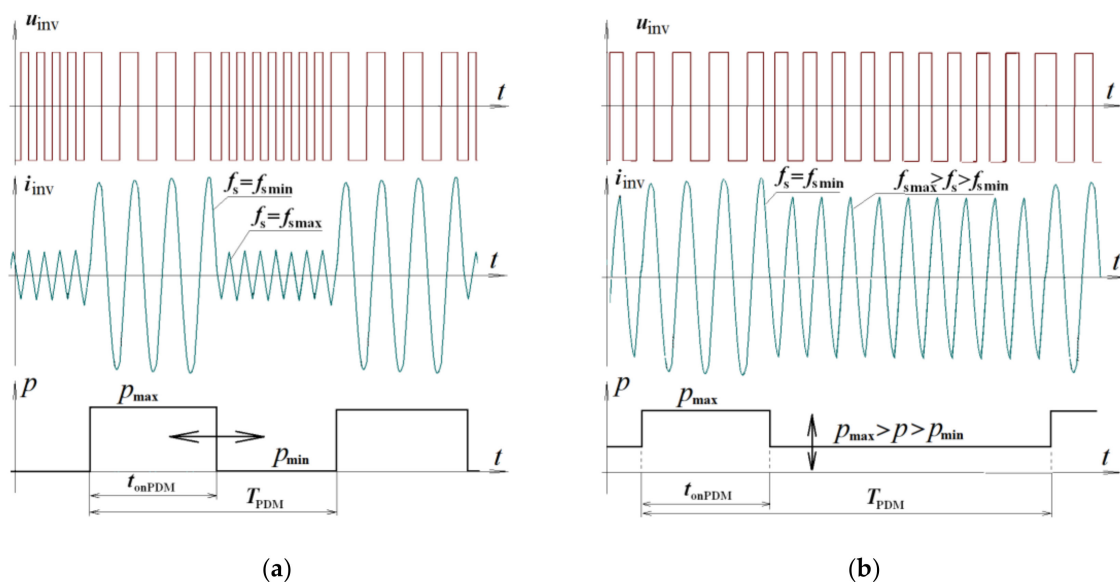


Figure 3. Examples of inverter output voltage and current waveforms using the PDM-PFM method developed by the authors: (a) with variable duty cycle of PDM signal, (b) at a constant duty cycle of PDM signal.

1.1.6. Choice of Control Method

In further projects and implementations, the PWM method was abandoned, because the inverter transistors could not work with ZVS soft commutation. The following methods were used to control HV generators for barrier discharges:

1. Power regulation by input voltage changes of the inverter (PAM, system with chopper) and switching of the inverter transistors with a frequency slightly higher than the resonant frequency. The switching frequency was tuned using the PLL loop. The inverter output voltage was ahead of the output current wave by approx. 2–3 μs . The inverter transistors switched under ZVS and almost ZCS conditions with very low commutation losses. This method of regulation ensured uniform discharges over the entire length of the electrodes in the range of 20–100% of the nominal power (P_N) of the device.
2. Power regulation by means of frequency modulation, above the resonant frequency (PFM, system without chopper), ensured the correct generation of DBD in the range of 20–100% of P_N . For a power lower than 20% of P_N , the system switched to PDM + PFM modulation according to the method developed by one of the authors. In this way, the power could be adjusted in the range of about 5–100% of P_N . This type of control ensured the operation of the inverter transistors in ZVS conditions.

2. Matching of HV Generators and DBD Reactors

Dielectric Barrier Discharges—Theoretical Basics

Figure 4 shows a simplified model of the discharge chamber. Figure 4a shows the construction ideas and Figure 4b presents simplified equivalent diagrams of the generator and the chamber. Figure 4b also contains the simplified characteristic of the barrier discharge in the air [21–24].

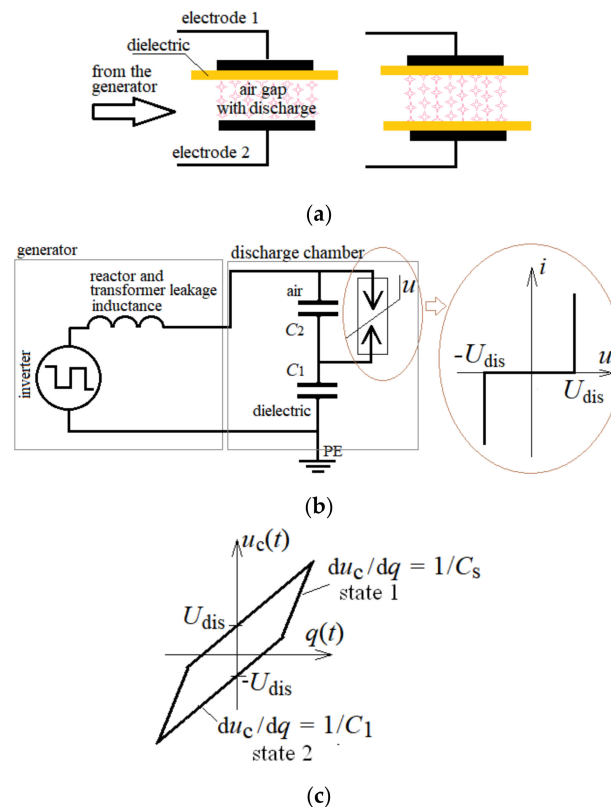


Figure 4. The idea of the construction of discharge chambers (a), simplified diagrams of the generator and the discharge chamber (b), and the trajectory of the voltage on the electrodes as a function of the charge supplied to these electrodes (c).

Capacities C_1 , C_2 and discharge (and ignition) voltage U_{dis} depend on the shape and size of the electrodes, dielectric thickness, and its type and width of the air gap [46]. Figure 4c shows the trajectory of the voltage on the electrodes as a function of the charge supplied to these electrodes. This trajectory allows determining the capacities of the equivalent diagram and ignition voltage. To design a device for generating DBD discharges, one needs to know the parameters of the discharge chamber, transformer ratio, voltage and frequency range of the inverter output voltage, inductance in the resonant circuit.

According to the simplified scheme and the $u_C(q)$ trajectory (Figure 4b,c) one can distinguish two states in chamber operation (Figure 4c): state 1, wherein there are no discharges and state 2 in which DBD discharges occur. In state 1 the increase rate du_C/dq on the chamber terminals depends on the substitute capacity C_S made up of series-connected capacitors C_1 and C_2 (3). In state 2 the capacitor C_2 voltage does not change and the du_C/dq depends on the C_1 capacity (4). Parameters of the discharge chamber can be experimentally determined based on $u_C(q)$ trajectory (Figure 4c).

$$\frac{du_C}{dq} = \frac{1}{C_S} = \frac{C_1 + C_2}{C_1 C_2} \quad (3)$$

$$\frac{du_C}{dq} = \frac{1}{C_1} \quad (4)$$

The chamber parameters related to the primary side of transformer are $C'_1 = \vartheta^2 C_1$, $C'_2 = \vartheta^2 C_2$, $C'_S = \vartheta^2 C_S$, $U_{\text{dis}} = U_{\text{dis}}/\vartheta$, where U_{dis} —discharge (and ignition) voltage, ϑ —transformation ratio. The frequency f_{syn} at which the inverter output voltage and current are synchronized is in the range $f_{r_{\text{max}}} > f_{\text{syn}} > f_{r_{\text{min}}}$ (Equations (5) and (6)) [34]. The synchronization frequency is the boundary of the transistors' abilities to work as ZVS or ZCS switches. The synchronization frequency f_{syn} at the rectangular inverter output voltage is only approximately equal to the resonant frequency [47].

$$f_{r_{\text{max}}} = \frac{1}{2\pi \sqrt{L_r C_S \vartheta^2}} \quad (5)$$

$$f_{r_{\text{min}}} = \frac{1}{2\pi \sqrt{L_r C_1 \vartheta^2}} \quad (6)$$

where $L_r = L_{\text{choke}} + L_\sigma$, L_{choke} —the additional choke (Figure 1) between the inverter output and the HV transformer, L_σ —the leakage inductance of the transformer seen from the low voltage side.

For the inverter voltage and frequency at which the capacitor C_2 voltage does not reach the U_{dis} , there are no discharges. In such conditions, the discharge chamber is a linear load. This creates a capacitor with a capacity of C_S . Capacitor C_S together with L_r creates a resonant circuit with low-pass filter properties. The shapes of electrode current and voltage are sinusoidal and the classical ac analysis can be used.

The amplitude of the capacitor C_2 voltage, which is referred to the first harmonic amplitude of the inverter output voltage is described by Equation (7), wherein $U_{C2_{1m}}$ —the amplitude of the capacitor C_2 voltage, $U_{\text{inv}_{1m}}$ —the first harmonic amplitude of the inverter output voltage (in the full bridge topology and a maximum duty cycle), $\omega_s = 2\pi f_s$ —circular frequency of the inverter output voltage, f_s —transistors switching frequency [24,34].

$$\frac{U_{C2_{1m}}/\vartheta}{U_{\text{inv}_{1m}}} = \left| \frac{1}{\omega_s^2 L_r \vartheta^2 C_S - 1} \cdot \frac{C_S}{C_2} \right| \quad (7)$$

where $U_{\text{inv}_{1m}} = \frac{4}{\pi} U_{\text{dc}}$, $U_{C2m} = U_{\text{dis}} \approx U_{C2_{1m}}$.

Equation (7) determines when the amplitude of the capacitor C_2 voltage reaches U_{dis} . The limit values of the switching frequencies at which the discharges appear, are determined based on Equations (8) and (9):

$$f_{s_lim_1} = \frac{1}{2\pi} \sqrt{\frac{1}{L_r \vartheta^2 C_2} \left(\frac{C_2}{C_S} - \frac{4}{\pi} \frac{U_{dc}}{U_{dis} / \vartheta} \right)} \quad (8)$$

$$f_{s_lim_2} = \frac{1}{2\pi} \sqrt{\frac{1}{L_r \vartheta^2 C_2} \left(\frac{C_2}{C_S} + \frac{4}{\pi} \frac{U_{dc}}{U_{dis} / \vartheta} \right)} \quad (9)$$

For PWM modulation, this equation is modified as shown in [29]. The discharges occur when $f_{s_lim_1} < f_s < f_{s_lim_2}$. The frequency limits depend on the capacity of the electrodes, the inductance of L_r , the discharge voltage, the inverter output voltage, and transformer winding ratio. The ratio of transformer winding has an impact on the operating frequency range and power of the device. By reducing the inverter output voltage these frequency limits approach to f_{r_max} (Equations (5) and (9)).

Figure 5a shows characteristics of discharges power as functions of frequency and inverter input voltage. Figure 5b illustrates power, current, and voltage characteristics as functions of frequency at a constant inverter input voltage (300 Vdc). Figure 5b illustrates the frequency limits according to the Equations (5), (6), (8), and (9). The characteristics from Figure 5a,b have been determined by assuming a constant value of the inductance L_r and transformer winding ratio. The following parameters of the real system (for treatment of plastic foil surface) were assumed in the simulation model: power $P_N = 3$ kW; $U_{dc} \approx 300$ V, two rotating electrodes: length 1700 mm, diameter 100 mm, 2 mm silicone insulation; two immovable electrodes: length 1600, width 36 mm toothed profile; air gap of approx. 2–4 mm (teeth); capacitance $C'_1 \approx 1.59$ nF, $C'_2 \approx 0.794$ nF; $L_r \approx 1.3$ mH; $\vartheta = 9.17$.

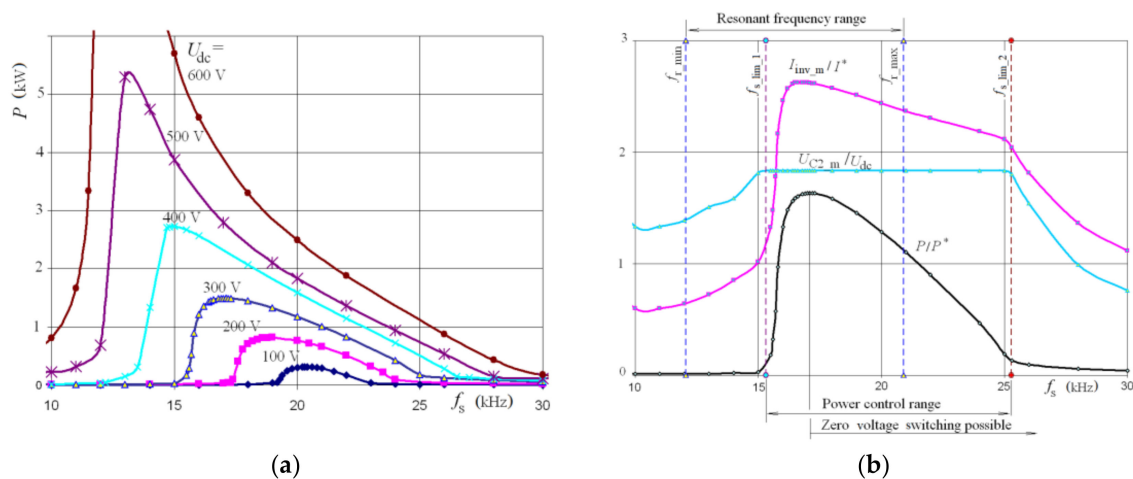


Figure 5. Characteristics of DBD discharges: (a) as a function of inverter output voltage and frequency, (b) as a function of inverter output frequency and constant inverter input voltage $U_{dc} = 300$ V, reproduced from Przegląd Elektrotechniczny [34]; the simulation results; base values: $I^* = U_{dc}/(L_r C_1')^{1/2}$, $P^* = U_{dc}^2/(L_r C_1')^{1/2}$.

Figure 6 shows the impact of the inductance and the transformation ratio on the frequency limits that define the range of switching frequency at the PFM modulation. The characteristics are derived by mathematical analysis (Equations (8) and (9)) for the above data. The same frequency limits were obtained by simulation. This is illustrated by the points on the curves in Figure 6. It is worth noting that experimentally measured frequencies did not diverge more than a few hundred Hz from those obtained by calculation and simulation.

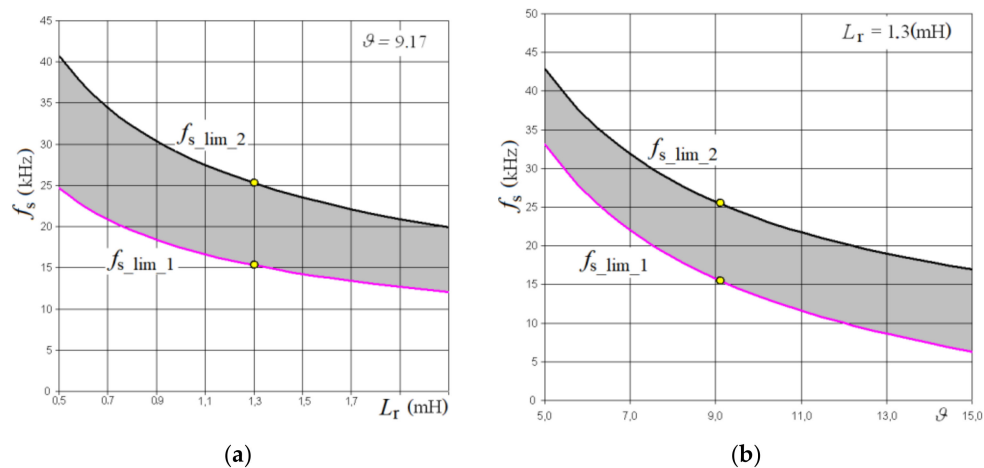


Figure 6. The range of the inverter output frequency at which the discharges appear (derived by mathematical analysis) as a function of: (a) inductance L_r ; (b) transformer windings ratio, reproduced from Przegląd Elektrotechniczny [34].

Increasing demand for processing different kinds of materials with different sizes generates the need to examine the impact of the transformer windings ratio and the inductance in the treatment process. Figure 7 presents the power control characteristics for the device with the same parameters as described above. The electrodes capacitance and voltage U_{dis} are fixed. Figure 7 shows that with a change of the transformation ratio the electrode capacities and voltage U_{dis} (referred to the inverter side) also change.

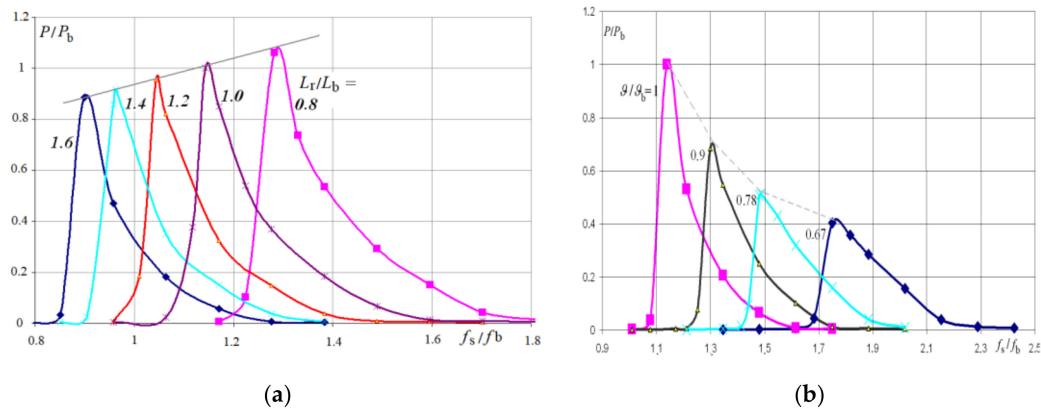


Figure 7. Relative discharge power as a function of frequency for: (a) various values of L_r ; (b) various values of ϑ , reproduced from Przegląd Elektrotechniczny [34]; base values: $L_b = 1$ mH, $\vartheta_b = 9.17$, $f_b = 1/(2\pi(C_1L_b)^{1/2})$.

3. Developed Prototype and Industrial Systems

3.1. Systems with Resonant Inverters for Surface Treatment (Activation) of Plastics

In order to modify the surface of plastics during printing, laminating, and gluing the DBD discharges (so-called corona treatment) are used. To achieve the desired level of adhesion the discharge energy in the range of 0.65–1.3 kJ/m² should be delivered. Parameters of HV generators for plastics surface treatment are generally in the range of power—0.5–10 kVA; frequency—5–50 kHz; voltage—4–20 kV. The schematic diagram of the power converter circuit used in the developed technological devices is shown in Figure 1. The idea of construction and the equivalent circuit of discharge chambers are presented in Figure 4a,b.

Figure 8 shows the construction principle of discharge chamber for foil processing, the trajectory $u(q)$ and waveforms of current, voltage, charge, and instantaneous power of the electrode set obtained experimentally. Discharges occur between the cylindrical (rotating) and rod electrode (Figure 8a). Capacitors assembly consists of the electrodes and two dielectric layers (silicon, quartz glass or ceramics, and air). The treated plastic makes the third layer of dielectric. Capacities of silicon and treated plastic foil are analyzed as one capacitor. Capacities of the electrodes and the leakage of transformer and additional choke inductances create a resonant circuit. The selection of transformer winding ratio and choke inductance allows for operating of the system in a given frequency range and assumed output power (Figures 5–7). The density of energy E/s (J/m^2) supplied to the plastic surface for the device as in Figure 8a can be determined from the equation:

$$E/s = P/(vd), \quad (10)$$

where P —DBD discharge power, v —speed of the foil, d —width of discharges (electrodes).

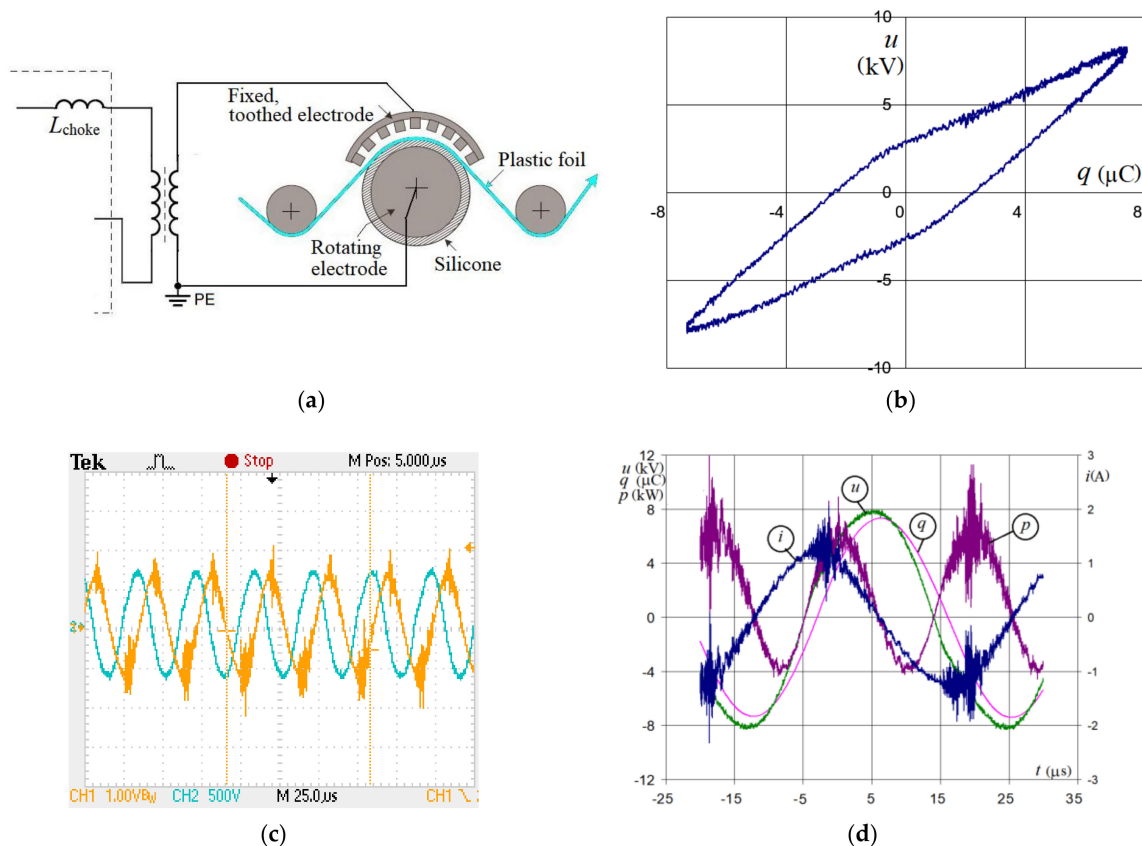


Figure 8. The discharge chamber for foil processing: (a) construction principle; (b) the trajectory $u(q)$ obtained experimentally at the frequency 26.8 kHz of the inverter output voltage and power 1.5 kW; (c) oscillogram of electrode current and voltage at the frequency of 26.8 kHz, CH1 1 A/div., CH2 6.25 kV/div.; (d) waveforms of current, voltage, charge, and instantaneous power of the electrode set obtained from the data from the oscillogram.

The waveforms of currents and voltages presented in Figure 8c were recorded using measuring devices: oscilloscope Tektronix TDS2024, current probe PA-622, high voltage differential probe P5200 with an additional voltage divider (1/12.5) at the input. The recorded data (from Figure 8c) were used to determine the trajectory from Figure 8b and the waveforms from Figure 8d. Excel was used for this purpose. The capacities of C_1 and C_2 were determined on the basis of the trajectory from Figure 8b and Equations (3) and (4). In order to determine the inductance $L_r = (L_{choke} + L_\sigma)$, the secondary winding

of the HV transformer was shorted and the additional choke and the transformer were powered from the inverter at reduced voltage. The rectangular voltage wave and the triangular current waveform at the inverter output were recorded. The inductance was determined on the basis of the relationship $L_T = U_{dc}(\Delta t/\Delta i)$ where Δt is half of the period of the inverter output voltage and Δi is the current increase during this time. The determined parameters values were used during the simulation, the results of which are shown in Figures 5–7. The dimensions of the discharge chamber and the determined parameters values can be found in the description of Figure 5.

The trajectory presented in Figure 8b prove that the model adopted for the analysis and simulation is correct for the averaged values of voltage and current of the electrodes. During the analysis and simulation with the use of this model, the electrodes current and power do not experience high-frequency oscillations visible in Figure 8c, d. This model can be used in the design and simplified analysis of the phenomena occurring in the discharge chamber. On the other hand, the oscillograms in Figure 8c, d show that many ignition and extinguishing processes occur simultaneously.

The generators for surface treatment of plastics by DBD discharge, which are described in this article, are produced now based on documentation and under the supervision of one of the authors at the Institute of Polymer Materials and Dyes Engineering (IMPiB, formerly Metalchem) in Torun, Poland [45]. Figure 9 presents the exemplary generator and discharge electrodes. The nominal powers of these generators in the range from 0.5 to 10 kW are produced.

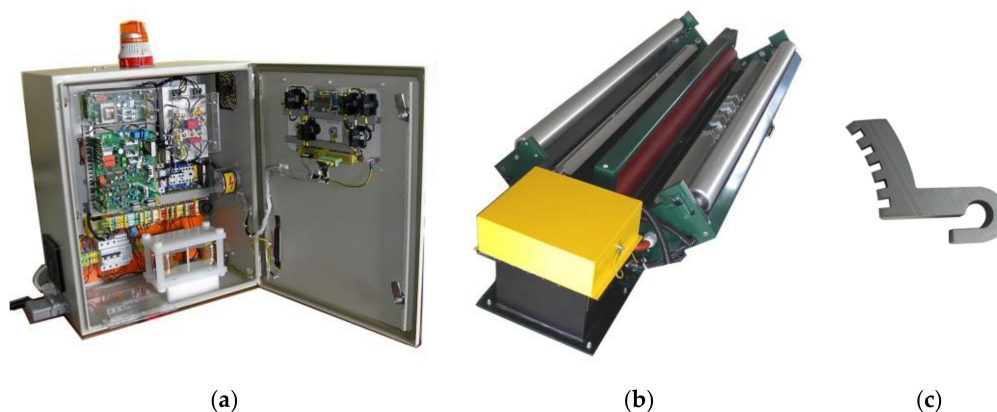


Figure 9. Construction of the devices for processing plastic film using DBD discharges: (a) power electronics generator with additional choke; (b) HV transformer and electrodes assembly, reproduced from web page IMPiB [45]; (c) part of the electrode.

3.2. Systems with Resonant Inverters for Decontamination of Loose Organic Material

Dielectric barrier discharges and ozone produced in this process can be used to decontaminate products such as seeds or ground dried plants. The use of plasma technologies in the food industry and agriculture has been described many times in literature [6,48–51]. However, these articles usually did not describe the construction details of plasma generators and reactors. Descriptions of some reactor designs can be found in patents [10,11]. The description of the DBD generation is analogous to the generation for surface treatment of plastics. However, the constructions of the discharge chambers are different. Figure 10 presents an equivalent diagram of part of the generator with HV transformer and construction of two types of discharge chambers for decontamination of loose organic material. The prototypes according to Figure 10b,c were built and tested under the supervision of one of the authors [7]. The first chamber (Figure 10b) has one fixed electrode, and the other in the form of a movable trolley that performs reciprocating movements transporting the treated organic material. The second version (Figure 10c) has two rotary electrodes in the form of cylinders between which the processed material is decontaminated.

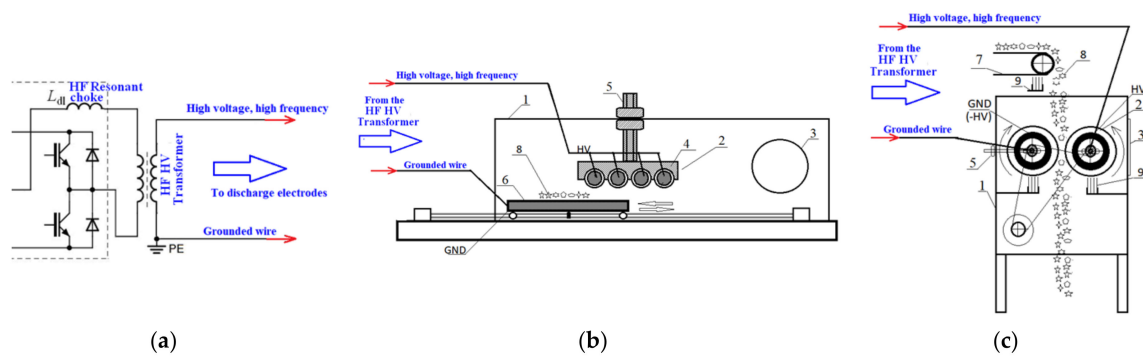


Figure 10. Construction of the devices for decontamination of loose organic material using DBD discharges: (a) equivalent diagram of part of a generator with transformer; (b) discharge chamber with a sliding electrode; (c) discharge chamber with rotating electrodes; 1—discharge chamber, 2—electrodes assembly, 3—suction hole, 4—insulating support, 5—electrodes gap adjustment knob, 6—transport trolley, 7—belt conveyor, 8—processed material, 9—sweeper.

New reactor designs were developed to increase the discharge power and thus to reduce the plasma exposure time and speed up the technological process. Plasma processing time is short compared with other known solutions [10]. Figure 11 shows two types of prototypes of devices for decontamination of crushed dried plants.

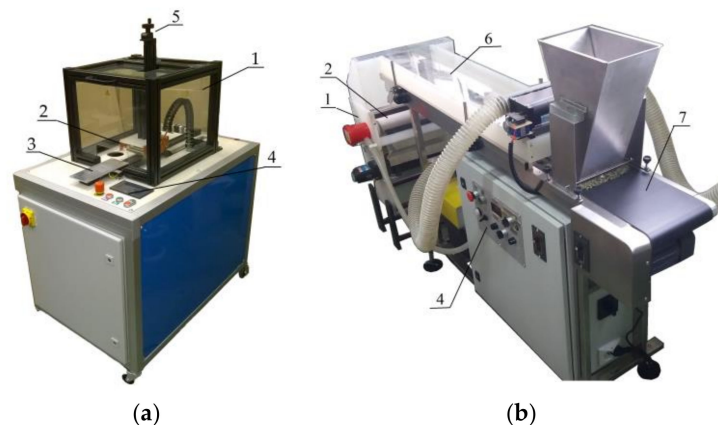


Figure 11. View of devices for decontamination of loose organic materials using DBD discharges developed and tested by the authors: (a) device with a sliding electrode; (b) device with rotating electrodes; 1—discharge chamber, 2—electrodes assembly, 3—transport trolley, 4—operator panel, 5—electrodes gap adjustment knob, 6—ozone chamber, 7—belt conveyor.

Figure 11b shows a solution that can be part of a technological line. This design is equipped with a support decontamination system which uses ozone generated in the discharge chamber. The conveyor speed determines the remaining time of the processed material in the ozone chamber. Electrodes in the form of rotating cylinders provide better cooling conditions than fixed electrodes. To increase the plasma operating time, the chamber may consist of several electrode assemblies. The implementation of such devices for the food industry is envisaged.

The power of discharges was regulated in the range of 200–1000 W by PFM or PDM + PFM modulation. The PDM + PFM modulation was used in the power range of 200–300 W to ensure even discharges over the entire length of the electrodes at low power. The decontamination efficiency of these prototypes was tested at the Faculty of Agriculture and Biotechnology of the UTP University in Bydgoszcz. The tests [52] confirm the effectiveness of DBD plasma and ozone in reducing microbial contamination of dried fragmented plants.

4. Conclusions

The article considers the most common problems concerning a proper matching of HV generators and DBD reactors. It focused on parameters of electrodes sets (equivalent capacitance, discharge voltage), generator parameters (frequency and output voltage, modulation methods), transformer parameters (transformation ratio, leakage inductances), and the resonant circuit choke inductance. Thus, the article contributes knowledge to designing equipment for surface treatment of plastics and for decontamination by DBD method.

A common feature of the presented systems is that the transistors of the inverters work with the ZVS soft commutation in the whole range of power regulation. In the case of PAM + PFM modulation, the transistors work with ZVS and "almost" ZCS commutation, which radically reduces switching losses. Resonant converters created in this way had better parameters than similar systems in which transistors operated with hard commutation. This concerned parameters such as efficiency and generation of radioelectric disturbances.

The innovative solutions presented in the article are the inverters for DBD plasma generators, which use the proprietary PDM + PFM modulation method. This method ensures the extension of the power regulation range and maintaining the uniformity of discharges in DBD devices for plastic surface treatment and decontamination. The generators were built using the theoretical considerations presented in this article. New designs of discharge chambers for decontamination have been developed. They have been reserved in the European patent office. The innovative solution of the first structure, with a movable GND electrode, is the ability to precisely select the dose of energy and decontamination conditions by adjusting the discharge power, the distance between the electrodes, the speed of the trolley with the GND electrode, the number of runs of the trolley during processing. An innovative solution of the second design is, among others, the use of rotating cylindrical electrodes, which improves cooling conditions and the use of ozone produced in the process for initial decontamination.

Author Contributions: Conceptualization, J.M.; methodology, J.M.; validation, J.M., R.S.; formal analysis, J.M., R.S.; investigation, J.M., R.D.; writing—original draft preparation, J.M.; writing—review and editing, R.S., R.D.; funding acquisition, J.M. All authors have read and agreed to the published version of the manuscript.

Funding: The mechanical design and construction of equipment for decontamination of loose plant products was financed by the UTP and UKW University consortium under the "Inkubator Innowacyjności Plus" project. Project application no. 17/02/2018/UTP. Other presented research received no external funding.

Acknowledgments: The authors would like to thank the employees of the Institute of Polymer Materials and Dyes Engineering (IMPIB) in Torun for their help and sharing of electrode sets and HV transformers. The authors also thank the staff of the Faculty of Agriculture and Biotechnology of the UTP University in Bydgoszcz for their help in evaluating the concept of devices for decontamination of loose organic materials.

Conflicts of Interest: The authors declare no conflict of interest.

References

1. Mittal, K.L.; Lyons, C.S. *Plasma Surface Modification of Polymers: Relevance to Adhesion*; Taylor & Francis Group: Abingdon, UK, 2019; p. 290. ISBN1 0367449463. ISBN2 9780367449469.
2. Nastuta, A.V.; Rusu, G.B.; Topala, I.; Chiper, A.; Popa, G. Surface modifications of polymer induced by atmospheric DBD plasma in different configurations. *J. Optoelectron. Adv. Mater.* **2008**, *10*, 2038–2042.
3. Santos, A.L.; Botelho, E.; Kostov, K.; Nascente, P.A.P.; Da Silva, L.L.G. Atmospheric plasma treatment of carbon fibers for enhancement of their adhesion properties. *IEEE Trans. Plasma Sci.* **2013**, *41*, 319–324. [[CrossRef](#)]
4. Kinnares, V.; Hothongkham, P. Circuit analysis and modeling of a phase-shifted pulsewidth modulation full-bridge-inverter-fed ozone generator with constant applied electrode voltage. *IEEE Trans. Power Electron.* **2010**, *25*, 1739–1752. [[CrossRef](#)]
5. Francke, K.-P.; Rudolph, R.; Miessner, H. Design and operating characteristics of a simple and reliable DBD reactor for use with atmospheric air. *Plasma Chem. Plasma Process.* **2003**, *23*, 47–57. [[CrossRef](#)]
6. Grabowski, M.; Holub, M.; Balcerak, M.; Kalisiak, S.; Dąbrowski, W. Black pepper powder microbiological quality improvement using DBD systems in atmospheric pressure. *Eur. Phys. J. Appl. Phys.* **2015**, *71*, 6. [[CrossRef](#)]

7. Mucko, J.; Panka, D.; Domanowski, P.; Bujnowski, S. Non-Thermal Plasma Reactor of Barrier Discharge for Disinfection and/or Sterilization of Organic Products. European. Patent Patent Application No. 20460005.0-1211, 29 January 2020.
8. Lin, C.M.; Chu, Y.C.; Hsiao, C.P.; Wu, J.S.; Hsieh, C.W.; Hou, C.Y. The optimization of plasma-activated water treatments to inactivate salmonella enteritidis (ATCC 13076) on shell eggs. *Foods* **2019**, *8*, 520. [[CrossRef](#)]
9. Ponomarev, A.V.; Gusev, A.I.; Pedos, M.S.; Sergeev, A.G.; Ustyuzhanin, A.V.; Podymova, A.S. High-Frequency Generator Based on Pulsed Excitation of the Oscillating Circuit for Biological Decontamination. In Proceedings of the IEEE International Conference on Plasma Science (ICOPS), San Francisco, CA, USA, 16–21 June 2013; p. 5. [[CrossRef](#)]
10. Grabowski, M.; Dąbrowski, W.; Balcerek, M.; Marcin, H.; Kalisiak, A.; Jakubowski, T.; Chyla, M. Reaktor Plazmy Nietermicznej do Sterylizacji Produktów Pochodzenia Organicznego. (Non-Thermal Plasma Reactor for Sterilizing Products of Organic Origin). U.S. Patent 2,307,98, 22 April 2015.
11. Heindl, A.; Müller, J.; Schulz, A.; Stroth, U.; Walker, M. Plasmaentkeimung. U.S. Patent DE 1,020,090,258,64A1, 14 October 2010.
12. Fridman, G.; Peddinghaus, M.; Fridman, A.; Balasubramanian, M.; Gutsol, A.; Friedman, G. Use of Non-Thermal Atmospheric Pressure Plasma Discharge for Coagulation and Sterilization of Surface Wounds. In Proceedings of the 17th International Conference on Plasma Chemistry, Toronto, ON, Canada, 7–12 August 2005; Paper No. 665. p. 6. [[CrossRef](#)]
13. Takayama, M.; Ebihara, K.; Stryczewska, H.; Ikegami, T.; Gyoutoku, Y.; Kubo, K.; Tachibana, M. *Ozone Generation by Dielectric Barrier Discharge for Soil Sterilization*; Elsevier: Amsterdam, The Netherlands, 2006; Volume 506–507, pp. 396–399. [[CrossRef](#)]
14. Oda, T.; Takahashi, T.; Nakano, H.; Masuda, S. Decomposition of fluorocarbon gaseous contaminants by surface discharge-induced plasma chemical processing. *IEEE Trans. Ind. Appl.* **1993**, *29*, 787–792. [[CrossRef](#)]
15. Yoshida, K. Aftertreatment of carbon particles emitted by diesel engine using a combination of corona and dielectric barrier discharge. *IEEE Trans. Ind. Appl.* **2019**, *55*, 5261–5268. [[CrossRef](#)]
16. Jakubowski, T.; Kalisiak, S.; Holub, M.; Palka, R.; Borkowski, T.; Myskow, J. New Resonant Inverter Topology with Active Energy Recovery in PDM Mode for DBD Plasma Reactor Supply. In Proceedings of the IEEE 14th European Conference on Power Electronics and Applications, Birmingham, UK, 30 August–1 September 2011; p. 8.
17. Du, Z.; Lin, X. Research Progress in Application of Low Temperature Plasma Technology for Wastewater Treatment. In Proceedings of the IOP Conference Series Earth and Environmental Science, Hangzhou, China, 17–19 April 2020; p. 7. [[CrossRef](#)]
18. Baloul, Y.; Aubry, O.; Rabat, H.; Colas, C.; Hong, D. Paracetamol degradation in aqueous solution by non-thermal plasma. *Eur. Phys. J. Appl. Phys.* **2017**, *79*. [[CrossRef](#)]
19. Holub, M.; Brandenburg, R.; Grosch, H.; Weinmann, S.; Hansel, B. Plasma supported odour removal from waste air in water treatment plants: An industrial case study. *Aerosol Air Qual. Res.* **2014**, *14*, 697–707. [[CrossRef](#)]
20. Holub, M.; Borkowski, T.; Jakubowski, T.; Kalisiak, S.; Myskow, J. Experimental results of a combined dbd reactor-catalyst assembly for a direct marine diesel-engine exhaust treatment. *IEEE Trans. Plasma Sci.* **2013**, *41*, 1562–1569. [[CrossRef](#)]
21. Kogelschatz, U. Dielectric-barrier discharges: Their history, discharge physics, and industrial applications. *Plasma Chem. Plasma Process.* **2003**, *23*, 1–46. [[CrossRef](#)]
22. Meißer, M. Resonant Behaviour of Pulse Generators for the Efficient Drive of Optical Radiation Sources Based on Dielectric Barrier Discharges. Ph.D. Thesis, Karlsruher Institut für Technologie, Karlsruhe, Germany, 2013. [[CrossRef](#)]
23. Rosenthal, L.A.; Davis, D.A. Electrical characterization of a corona discharge for surface treatment. *IEEE Trans. Ind. Appl.* **1975**, *11*, 328–335. [[CrossRef](#)]
24. Mucko, J. Corona Treatment System with Resonant Inverter-Selected Properties. In Proceedings of the 13th International Power Electronics and Motion Control Conference (EPE-PEMC), Poznan, Poland, 1–3 September 2008; pp. 1339–1343. [[CrossRef](#)]
25. Mehmood, A.; Jamal, H. Analysis on the Propulsion of Ionic Wind During Corona Discharge in Various Electrode Configuration with High Voltage Sources. In Proceedings of the IEEE International Conference on Applied and Engineering Mathematics (ICAEM), Taxila, Pakistan, 27–29 August 2019. [[CrossRef](#)]

26. Sosa, R.; Grondona, D.; Márquez, A.; Artana, G.; Kelly, H. On the induced gas flow by a trielectrode plasma curtain at atmospheric pressure. *IEEE Trans. Ind. Appl.* **2010**, *46*, 1132–1137. [[CrossRef](#)]
27. Siemens, W. Ueber die elektrostatische induction und die verzögerung des stroms in flaschendrähnen. *Ann. Phys.* **1857**, *178*, 66–122. [[CrossRef](#)]
28. Pekarek, S. DC corona ozone generation enhanced by TiO₂ photocatalyst. *Eur. Phys. J. D* **2008**, *50*, 171–175. [[CrossRef](#)]
29. Tsai, M.T.; Ke, C.W. Design and Implementation of a High-Voltage High-Frequency Pulse Power Generation System for Plasma Applications. In Proceedings of the International Conference on Power Electronics and Drive Systems (PEDS), Taipei, Taiwan, 2–5 November 2009; pp. 1556–1560. [[CrossRef](#)]
30. Tsai, M.T.; Chu, C.L. Power Control Strategies Evaluation of a Series Resonant Inverter for Atmosphere Plasma Applications. In Proceedings of the IEEE International Symposium on Industrial Electronics (ISIE), Seoul, Korea, 5–8 July 2009; pp. 632–637. [[CrossRef](#)]
31. Liu, Y.; He, X. A Series Resonant Inverter System with PDM and PFM hybrid Control for Plastic Film Surface Treatment. In Proceedings of the Industry Applications Conference (IAS), Hong Kong, China, 2–6 October 2005; pp. 1700–1704. [[CrossRef](#)]
32. Liu, Y.; He, X. PDM and PFM hybrid control of a series-resonant inverter for corona surface treatment. *IEE Proc. Electr. Power Appl.* **2005**, *152*, 1445. [[CrossRef](#)]
33. Luan, S.; Tang, X.; Wang, L.; Chen, S. Research of Phase-Shift Series-Load Resonant Power Supply for DBD-Ozone Generator. In Proceedings of the 6th International Conference on Power Electronics Systems and Applications (PESA), Hong Kong, China, 15–17 December 2015; p. 7. [[CrossRef](#)]
34. Mucko, J. Influence of the inverter output circuit on the dielectric barrier discharges during the surface treatment of plastics. *Prz. Elektrotechn. (Electrotech. Rev.)* **2015**, *91*, 95–98. [[CrossRef](#)]
35. Mucko, J. Aktywator folii z falownikiem rezonansowym - właściwości, metody i układy sterowania. (Corona treatment with resonant inverter-propriety, control methods and circuits). *Prz. Elektrotechn. (Electrotech. Rev.)* **2005**, *81*, 42–49.
36. Changsheng, H.; Yushui, H.; Liqiao, W.; Zhongchao, Z. A Closed-loop Control for the Power Source of the Ozonizer. In Proceedings of the 35th Annual IEEE Power Electronics Specialists Conference, Aachen, Germany, 20–25 June 2004; pp. 3984–3987. [[CrossRef](#)]
37. Kalisiak, S.; Hołub, M.; Jakubowski, T. Resonant Inverter with Output Voltage Pulse-Phase-Shift Control for DBD Plasma Reactor Supply. In Proceedings of the 13th European Conference on Power Electronics and Applications, Barcelona, Spain, 8–10 September 2009; p. 9.
38. Kalisiak, S.; Jakubowski, T.; Holub, M. Single-Period AC Source with Energy Transfer Control for Dielectric Barrier Discharge Plasma Applications. In Proceedings of the 14th International Power Electronics and Motion Control Conference, EPE-PEMC, Ohrid, Macedonia, 6–8 September 2010; pp. 103–109. [[CrossRef](#)]
39. Dragonas, F.A.; Grandi, G.; Neretti, G. High-Voltage High-Frequency Arbitrary Waveform Multilevel Generator for Dielectric Barrier Discharge. In Proceedings of the International Symposium on Power Electronics, Electrical Drives, Automation and Motion, Ischia, Italy, 18–20 June 2014; pp. 57–61. [[CrossRef](#)]
40. Dragonas, F.A.; Neretti, G.; Sanjeevikumar, P.; Grandi, G. High-voltage high-frequency arbitrary waveform multilevel generator for dbd plasma actuators. *IEEE Trans. Ind. Appl.* **2015**, *51*, 3334–3342. [[CrossRef](#)]
41. Burány, N.; Huber, L.; Pejovic, P. Corona discharge surface treater without high voltage transformer. *IEEE Trans. Power Electron.* **2008**, *23*, 993–1002. [[CrossRef](#)]
42. Mućko, J.; Strzelecki, R.; Kozakiewicz, J.; Lutomirski, S. Resonant Inverters with Improved Output Characteristics in Application for Corona Discharge Treatment. In Proceedings of the European Conference on Power Electronics and Applications (EPE'99), Lausanne, Switzerland, 7–9 September 1999; pp. 1–6, Paper no. 857.
43. Fujita, H.; Ogasawara, S.; Akagi, H. An Approach to Broad Range of Power Control in Voltage-Source Series-Resonant Inverters for Corona Discharge Treatment. In Proceedings of the IEEE Power Electronics Specialists Conference (PESC), Saint Louis, MO, USA, 22–27 June 1997; pp. 1000–1006. [[CrossRef](#)]
44. Mućko, J. Control Method of Resonant Inverter for Application of a Foil Treatment (Sposób Sterowania Falownikiem Rezonansowym w Zastosowaniu Aktywatora Folii). Polish Patent No. 384865, 7 April 2008.
45. Instytut Inżynierii Materiałów Polimetyowych i Barwników (Institute of Polymer Materials and Dyes Engineering), Torun, Poland, Selected Constructions of the Implemented Devices. Available online: <http://www.torun.impib.pl/oferta/oferta-urzadzen-i-maszyn/aktywatory> (accessed on 4 August 2020).

46. Meek, J.; Craggs, J. *Electrical Breakdown of Gases*; John Wiley & Sons: New York, NY, USA, 1978.
47. Mucko, J.; Strzelecki, R. Errors in the Analysis of Series Resonant Inverter/Converter Assuming Sinusoidal Waveforms of Voltage and Current. In Proceedings of the 10th International Conference on Compatibility, Power Electronics and Power Engineering (CPE-POWERENG), Bydgoszcz, Poland, 29 June–1 July 2016; pp. 369–374. [[CrossRef](#)]
48. Misra, N.N.; Schluter, O.; Cullen, P.J. *Cold Plasma in Food and Agriculture: Fundamentals and Applications*; Academic Press: Cambridge, MA, USA, 2016; p. 380. ISBN 9780128014899.
49. Santos, L.C.O.; Vieira, A.L.; Moecke, E.H.S.; Ribeiro, D.H.B.; Amante, E.R. Use of cold plasma to inactivate escherichia coli and physicochemical evaluation in pumpkin puree. *J. Food Prot.* **2018**, *81*, 1897–1905. [[CrossRef](#)] [[PubMed](#)]
50. Pankaj, S.; Wan, Z.; Keener, K.M. Effects of cold plasma on food quality: A review. *Foods* **2018**, *7*, 4. [[CrossRef](#)]
51. Han, L.; Patil, S.; Boehm, D.; Milosavljević, V.; Cullen, P.J.; Bourke, P. Mechanisms of inactivation by high-voltage atmospheric cold plasma differ for escherichia coli and staphylococcus aureus. *Appl. Environ. Microbiol.* **2016**, *82*, 450–458. [[CrossRef](#)]
52. Panka, D.; Jeske, M.; Lisiecki, K.; Mucko, J. Research on use of Cold Plasma for Disinfection of Plant Material. In Proceedings of the 4th World Summit & Expo on Food Technology and Probiotics, Bangkok, Thailand, 24–25 October 2019; p. 29.



© 2020 by the authors. Licensee MDPI, Basel, Switzerland. This article is an open access article distributed under the terms and conditions of the Creative Commons Attribution (CC BY) license (<http://creativecommons.org/licenses/by/4.0/>).